Measurements of the absolute branching fractions of hadronic *D*-meson decays involving kaons and pions

M. Ablikim,[1] M. N. Achasov,[10,b] P. Adlarson,[69] S. Ahmed,[15] M. Albrecht,[4] R. Aliberti,[29] A. Amoroso,[68a,68c] M. R. An,[33] Q. An,[65,51] X. H. Bai,[59] Y. Bai,[50] O. Bakina,[30] R. Baldini Ferroli,[24a] I. Balossino,[25a] Y. Ban,[40,g] K. Begzsuren,[27] N. Berger,[29] M. Bertani,[24a] D. Bettoni,[25a] F. Bianchi,[68a,68c] J. Bloms,[62] A. Bortone,[68a,68c] I. Boyko,[30] R. A. Briere,[5] A. Brueggemann,[62] H. Cai,[70] X. Cai,[1,51] A. Calcaterra,[24a] G. F. Cao,[1,56] N. Cao,[1,56] S. A. Cetin,[55a] J. F. Chang,[1,51] W. L. Chang,[1,56] G. Chelkov,[30,a] G. Chen,[1] H. S. Chen,[1,56] M. L. Chen,[1,51] S. J. Chen,[36] X. R. Chen,[26,56] Y. B. Chen,[1,51] Z. J. Chen,[21,h] W. S. Cheng,[68c] G. Cibinetto,[25a] F. Cossio,[68c] J. J. Cui,[43] H. L. Dai,[1,51] J. P. Dai,[72] A. Dbeyssi,[15] R. E. de Boer,[4] D. Dedovich,[30] Z. Y. Deng,[1] A. Denig,[29] I. Denysenko,[30] M. Destefanis,[68a,68c] F. De Mori,[68a,68c] Y. Ding,[34] J. Dong,[1,51] L. Y. Dong,[1,56] M. Y. Dong,[1,51,56] X. Dong,[70] S. X. Du,[74] Y. L. Fan,[70] J. Fang,[1,51] S. S. Fang,[1,56] Y. Fang,[1] R. Farinelli,[25a] L. Fava,[68b,68c] F. Feldbauer,[4] G. Felici,[24a] C. Q. Feng,[65,51] J. H. Feng,[52] M. Fritsch,[4] C. D. Fu,[1] H. Gao,[56] Y. N. Gao,[40,g] Yang Gao,[65,51] I. Garzia,[25a,25b] P. T. Ge,[70] Z. W. Ge,[36] C. Geng,[52] E. M. Gersabeck,[60] A. Gilman,[63] K. Goetzen,[11] L. Gong,[34] W. X. Gong,[1,51] W. Gradl,[29] M. Greco,[68a,68c] L. M. Gu,[36] M. H. Gu,[1,51] Y. T. Gu,[13] C. Y. Guan,[1,56] A. Q. Guo,[26,56] L. B. Guo,[35] R. P. Guo,[42] Y. P. Guo,[9,f] A. Guskov,[30,a] T. T. Han,[43] W. Y. Han,[33] X. Q. Hao,[16] F. A. Harris,[58] K. L. He,[1,56] F. H. Heinsius,[4] C. H. Heinz,[29] Y. K. Heng,[1,51,56] C. Herold,[53] M. Himmelreich,[11,d] T. Holtmann,[4] G. Y. Hou,[1,56] Y. R. Hou,[56] Z. L. Hou,[1] H. M. Hu,[1,56] J. F. Hu,[49,i] T. Hu,[1,51,56] Y. Hu,[1] G. S. Huang,[65,51] L. Q. Huang,[66] X. T. Huang,[43] Y. P. Huang,[1] Z. Huang,[40,g] T. Hussain,[67] N. Hüsken,[23,29] W. Imoehl,[23] M. Irshad,[65,51] J. Jackson,[23] S. Jaeger,[4] S. Janchiv,[27] Q. Ji,[1] Q. P. Ji,[16] X. B. Ji,[1,56] X. L. Ji,[1,51] Y. Y. Ji,[43] H. B. Jiang,[43] X. S. Jiang,[1,51,56] Y. Jiang,[56] J. B. Jiao,[43] Z. Jiao,[19] S. Jin,[36] Y. Jin,[59] M. Q. Jing,[1,56] T. Johansson,[69] N. Kalantar-Nayestanaki,[57] X. S. Kang,[34] R. Kappert,[57] M. Kavatsyuk,[57] B. C. Ke,[45,1] I. K. Keshk,[4] A. Khoukaz,[62] P. Kiese,[29] R. Kiuchi,[1] R. Kliemt,[11] L. Koch,[31] O. B. Kolcu,[55a] B. Kopf,[4] M. Kuemmel,[4] M. Kuessner,[4] A. Kupsc,[38,69] W. Kühn,[31] J. J. Lane,[60] J. S. Lange,[31] P. Larin,[15] A. Lavania,[22] L. Lavezzi,[68a,68c] Z. H. Lei,[65,51] H. Leithoff,[29] M. Lellmann,[29] T. Lenz,[29] C. Li,[41] C. H. Li,[33] Cheng Li,[65,51] D. M. Li,[74] F. Li,[1,51] G. Li,[1] H. Li,[65,51] H. Li,[45] H. B. Li,[1,56] H. J. Li,[16] H. N. Li,[49,i] L. X. Li,[37] J. Q. Li,[4] J. S. Li,[52] J. W. Li,[43] Ke Li,[1] L. K. Li,[1] Lei Li,[3] P. R. Li,[32,j,k] S. Y. Li,[54] T. Li,[43] W. D. Li,[1,56] W. G. Li,[1] X. H. Li,[65,51] X. L. Li,[43] Xiaoyu Li,[1,56] H. Liang,[65,51] H. Liang,[28] H. Liang,[1,56] Y. F. Liang,[47] Y. T. Liang,[26,56] G. R. Liao,[12] L. Z. Liao,[43] J. Libby,[22] A. Limphirat,[53] C. X. Lin,[52] D. X. Lin,[26,56] T. Lin,[1] B. J. Liu,[1] C. X. Liu,[1] D. Liu,[15,65] F. H. Liu,[46] Fang Liu,[1] Feng Liu,[6] G. M. Liu,[49,i] H. B. Liu,[13] H. M. Liu,[1,56] Huanhuan Liu,[1] Huihui Liu,[17] J. B. Liu,[65,51] J. L. Liu,[66] J. Y. Liu,[1,56] K. Liu,[1] K. Y. Liu,[34] Ke Liu,[18] L. Liu,[65,51] Lu Liu,[37] M. H. Liu,[9,f] P. L. Liu,[1] Q. Liu,[56] Q. Liu,[70] S. B. Liu,[65,51] T. Liu,[9,f] W. K. Liu,[37] W. M. Liu,[65,51] X. Liu,[32,j,k] Y. Liu,[32,j,k] Y. B. Liu,[37] Z. A. Liu,[1,51,56] Z. Q. Liu,[43] X. C. Lou,[1,51,56] F. X. Lu,[52] H. J. Lu,[19] J. G. Lu,[1,51] X. L. Lu,[1] Y. Lu,[1] Y. P. Lu,[1,51] C. L. Luo,[35] M. X. Luo,[73] T. Luo,[9,f] X. L. Luo,[1,51] X. R. Lyu,[56] F. C. Ma,[34] H. L. Ma,[1] L. L. Ma,[43] M. M. Ma,[1,56] Q. M. Ma,[1] R. Q. Ma,[1,56] R. T. Ma,[56] X. Y. Ma,[1,51] Y. Ma,[40,g] F. E. Maas,[15] M. Maggiora,[68a,68c] S. Maldaner,[4] S. Malde,[63] Q. A. Malik,[67] A. Mangoni,[24b] Y. J. Mao,[40,g] Z. P. Mao,[1] S. Marcello,[68a,68c] Z. X. Meng,[59] J. G. Messchendorp,[57,11] G. Mezzadri,[25a] T. J. Min,[36] R. E. Mitchell,[23] X. H. Mo,[1,51,56] N. Yu. Muchnoi,[10,b] H. Muramatsu,[61] S. Nakhoul,[11,d] Y. Nefedov,[30] F. Nerling,[11,d] I. B. Nikolaev,[10,b] Z. Ning,[1,51] S. Nisar,[8,l] S. L. Olsen,[56] Q. Ouyang,[1,51,56] S. Pacetti,[24b,24c] X. Pan,[9,f] Y. Pan,[60] A. Pathak,[28] P. Patteri,[24a] M. Pelizaeus,[4] H. P. Peng,[65,51] K. Peters,[11,d] J. L. Ping,[35] R. G. Ping,[1,56] S. Pogodin,[30] R. Poling,[61] V. Prasad,[65,51] H. Qi,[65,51] H. R. Qi,[54] M. Qi,[36] T. Y. Qi,[9,f] S. Qian,[1,51] W. B. Qian,[56] Z. Qian,[52] C. F. Qiao,[56] J. J. Qin,[66] L. Q. Qin,[12] X. P. Qin,[9,f] X. S. Qin,[43] Z. H. Qin,[1,51] J. F. Qiu,[1] S. Q. Qu,[54] K. H. Rashid,[67] K. Ravindran,[22] C. F. Redmer,[29] A. Rivetti,[68c] V. Rodin,[57] M. Rolo,[68c] G. Rong,[1,56] Ch. Rosner,[15] H. S. Sang,[65] A. Sarantsev,[30,c] Y. Schelhaas,[29] C. Schnier,[4] K. Schoenning,[69] M. Scodeggio,[25a,25b] W. Shan,[20] X. Y. Shan,[65,51] J. F. Shangguan,[48] M. Shao,[65,51] C. P. Shen,[9,f] H. F. Shen,[1,56] X. Y. Shen,[1,56] H. C. Shi,[65,51] R. S. Shi,[1,56] X. Shi,[1,51] X. D. Shi,[65,51] J. J. Song,[16] W. M. Song,[28,1] Y. X. Song,[40,g] S. Sosio,[68a,68c] S. Spataro,[68a,68c] K. X. Su,[70] P. P. Su,[48] G. X. Sun,[1] H. K. Sun,[1] J. F. Sun,[16] L. Sun,[70] S. S. Sun,[1,56] T. Sun,[1,56] W. Y. Sun,[28] X. Sun,[21,h] Y. J. Sun,[65,51] Y. Z. Sun,[1] Z. T. Sun,[43] Y. H. Tan,[70] Y. X. Tan,[65,51] C. J. Tang,[47] G. Y. Tang,[1] J. Tang,[52] J. X. Teng,[65,51] V. Thoren,[69] W. H. Tian,[45] Y. Tian,[26,56] I. Uman,[55b] B. Wang,[1] B. L. Wang,[56] C. W. Wang,[36] D. Y. Wang,[40,g] H. J. Wang,[32,j,k] H. P. Wang,[1,56] K. Wang,[1,51] L. L. Wang,[1] M. Wang,[43] M. Z. Wang,[40,g] Meng Wang,[1,56] S. Wang,[9,f] W. Wang,[52] W. H. Wang,[70] W. P. Wang,[65,51] X. Wang,[40,g] X. F. Wang,[32,j,k] X. L. Wang,[9,f] Y. D. Wang,[39] Y. F. Wang,[1,51,56] Y. Q. Wang,[1] Z. Wang,[1,51] Z. Y. Wang,[1,56] Ziyi Wang,[56] D. H. Wei,[12] F. Weidner,[62] S. P. Wen,[1] D. J. White,[60] U. Wiedner,[4] G. Wilkinson,[63] M. Wolke,[69] L. Wollenberg,[4] J. F. Wu,[1,56] L. H. Wu,[1] L. J. Wu,[1,56] X. Wu,[9,f] X. H. Wu,[28] Y. Wu,[65] Z. Wu,[1,51] L. Xia,[65,51] T. Xiang,[40,g] G. Y. Xiao,[36] H. Xiao,[9,f] S. Y. Xiao,[1] Z. J. Xiao,[35] C. Xie,[36] X. H. Xie,[40,g] Y. Xie,[43] Y. G. Xie,[1,51] Y. H. Xie,[6] Z. P. Xie,[65,51] T. Y. Xing,[1,56] C. J. Xu,[52] G. F. Xu,[1] Q. J. Xu,[14] X. P. Xu,[48] Y. C. Xu,[56] Z. P. Xu,[36] F. Yan,[9,f] L. Yan,[9,f] W. B. Yan,[65,51] W. C. Yan,[74] H. J. Yang,[44,e] H. X. Yang,[1] L. Yang,[45] S. L. Yang,[56] Yifan Yang,[1,56] Zhi Yang,[26] M. Ye,[1,51] M. H. Ye,[7] J. H. Yin,[1] Z. Y. You,[52] B. X. Yu,[1,51,56] C. X. Yu,[37] G. Yu,[1,56] J. S. Yu,[21,h] T. Yu,[66] C. Z. Yuan,[1,56] L. Yuan,[2] X. Q. Yuan,[1]

Y. Yuan,[1,56] Z. Y. Yuan,[52] C. X. Yue,[33] A. A. Zafar,[67] X. Zeng Zeng,[6] Y. Zeng,[21,h] A. Q. Zhang,[1] B. X. Zhang,[1] G. Y. Zhang,[16] H. Zhang,[65] H. H. Zhang,[52] H. H. Zhang,[28] H. Y. Zhang,[1,51] J. L. Zhang,[71] J. Q. Zhang,[35] J. W. Zhang,[1,51,56] J. Y. Zhang,[1] J. Z. Zhang,[1,56] Jianyu Zhang,[1,56] Jiawei Zhang,[1,56] L. M. Zhang,[54] L. Q. Zhang,[52] Lei Zhang,[36] S. F. Zhang,[36] Shulei Zhang,[21,h] X. D. Zhang,[39] X. Y. Zhang,[43] Y. Zhang,[63] Y. T. Zhang,[74] Y. H. Zhang,[1,51] Yan Zhang,[65,51] Yao Zhang,[1] Z. Y. Zhang,[70] G. Zhao,[1] J. Zhao,[33] J. Y. Zhao,[1,56] J. Z. Zhao,[1,51] Lei Zhao,[65,51] Ling Zhao,[1] M. G. Zhao,[37] Q. Zhao,[1] S. J. Zhao,[74] Y. B. Zhao,[1,51] Y. X. Zhao,[26,56] Z. G. Zhao,[65,51] A. Zhemchugov,[30,a] B. Zheng,[66] J. P. Zheng,[1,51] Y. H. Zheng,[56] B. Zhong,[35] C. Zhong,[66] H. Zhou,[43] L. P. Zhou,[1,56] X. Zhou,[70] X. K. Zhou,[56] X. R. Zhou,[65,51] X. Y. Zhou,[33] J. Zhu,[37] K. Zhu,[1] K. J. Zhu,[1,51,56] L. X. Zhu,[56] S. H. Zhu,[64] S. Q. Zhu,[36] T. J. Zhu,[71] W. J. Zhu,[9,f] Y. C. Zhu,[65,51] Z. A. Zhu,[1,56] B. S. Zou,[1] and J. H. Zou[1]

(BESIII Collaboration)

[1]*Institute of High Energy Physics, Beijing 100049, People's Republic of China*
[2]*Beihang University, Beijing 100191, People's Republic of China*
[3]*Beijing Institute of Petrochemical Technology, Beijing 102617, People's Republic of China*
[4]*Bochum Ruhr-University, D-44780 Bochum, Germany*
[5]*Carnegie Mellon University, Pittsburgh, Pennsylvania 15213, USA*
[6]*Central China Normal University, Wuhan 430079, People's Republic of China*
[7]*China Center of Advanced Science and Technology, Beijing 100190, People's Republic of China*
[8]*COMSATS University Islamabad, Lahore Campus, Defence Road, Off Raiwind Road,
54000 Lahore, Pakistan*
[9]*Fudan University, Shanghai 200433, People's Republic of China*
[10]*G.I. Budker Institute of Nuclear Physics SB RAS (BINP), Novosibirsk 630090, Russia*
[11]*GSI Helmholtzcentre for Heavy Ion Research GmbH, D-64291 Darmstadt, Germany*
[12]*Guangxi Normal University, Guilin 541004, People's Republic of China*
[13]*Guangxi University, Nanning 530004, People's Republic of China*
[14]*Hangzhou Normal University, Hangzhou 310036, People's Republic of China*
[15]*Helmholtz Institute Mainz, Staudinger Weg 18, D-55099 Mainz, Germany*
[16]*Henan Normal University, Xinxiang 453007, People's Republic of China*
[17]*Henan University of Science and Technology, Luoyang 471003, People's Republic of China*
[18]*Henan University of Technology, Zhengzhou 450001, People's Republic of China*
[19]*Huangshan College, Huangshan 245000, People's Republic of China*
[20]*Hunan Normal University, Changsha 410081, People's Republic of China*
[21]*Hunan University, Changsha 410082, People's Republic of China*
[22]*Indian Institute of Technology Madras, Chennai 600036, India*
[23]*Indiana University, Bloomington, Indiana 47405, USA*
[24a]*INFN Laboratori Nazionali di Frascati, I-00044 Frascati, Italy*
[24b]*INFN Sezione di Perugia, I-06100 Perugia, Italy*
[24c]*University of Perugia, I-06100 Perugia, Italy*
[25a]*INFN Sezione di Ferrara, I-44122 Ferrara, Italy*
[25b]*University of Ferrara, I-44122 Ferrara, Italy*
[26]*Institute of Modern Physics, Lanzhou 730000, People's Republic of China*
[27]*Institute of Physics and Technology, Peace Avenue 54B, Ulaanbaatar 13330, Mongolia*
[28]*Jilin University, Changchun 130012, People's Republic of China*
[29]*Johannes Gutenberg University of Mainz, Johann-Joachim-Becher-Weg 45, D-55099 Mainz, Germany*
[30]*Joint Institute for Nuclear Research, 141980 Dubna, Moscow region, Russia*
[31]*Justus-Liebig-Universitaet Giessen, II. Physikalisches Institut, Heinrich-Buff-Ring 16,
D-35392 Giessen, Germany*
[32]*Lanzhou University, Lanzhou 730000, People's Republic of China*
[33]*Liaoning Normal University, Dalian 116029, People's Republic of China*
[34]*Liaoning University, Shenyang 110036, People's Republic of China*
[35]*Nanjing Normal University, Nanjing 210023, People's Republic of China*
[36]*Nanjing University, Nanjing 210093, People's Republic of China*
[37]*Nankai University, Tianjin 300071, People's Republic of China*
[38]*National Centre for Nuclear Research, Warsaw 02-093, Poland*
[39]*North China Electric Power University, Beijing 102206, People's Republic of China*
[40]*Peking University, Beijing 100871, People's Republic of China*
[41]*Qufu Normal University, Qufu 273165, People's Republic of China*
[42]*Shandong Normal University, Jinan 250014, People's Republic of China*

[43]*Shandong University, Jinan 250100, People's Republic of China*
[44]*Shanghai Jiao Tong University, Shanghai 200240, People's Republic of China*
[45]*Shanxi Normal University, Linfen 041004, People's Republic of China*
[46]*Shanxi University, Taiyuan 030006, People's Republic of China*
[47]*Sichuan University, Chengdu 610064, People's Republic of China*
[48]*Soochow University, Suzhou 215006, People's Republic of China*
[49]*South China Normal University, Guangzhou 510006, People's Republic of China*
[50]*Southeast University, Nanjing 211100, People's Republic of China*
[51]*State Key Laboratory of Particle Detection and Electronics, Beijing 100049, Hefei 230026,*
People's Republic of China
[52]*Sun Yat-Sen University, Guangzhou 510275, People's Republic of China*
[53]*Suranaree University of Technology, University Avenue 111, Nakhon Ratchasima 30000, Thailand*
[54]*Tsinghua University, Beijing 100084, People's Republic of China*
[55a]*Turkish Accelerator Center Particle Factory Group, Istinye University, 34010 Istanbul, Turkey*
[55b]*Near East University, Nicosia, North Cyprus, Mersin 10 99138, Turkey*
[56]*University of Chinese Academy of Sciences, Beijing 100049, People's Republic of China*
[57]*University of Groningen, NL-9747 AA Groningen, Netherlands*
[58]*University of Hawaii, Honolulu, Hawaii 96822, USA*
[59]*University of Jinan, Jinan 250022, People's Republic of China*
[60]*University of Manchester, Oxford Road, Manchester M13 9PL, United Kingdom*
[61]*University of Minnesota, Minneapolis, Minnesota 55455, USA*
[62]*University of Muenster, Wilhelm-Klemm-Strasse 9, 48149 Muenster, Germany*
[63]*University of Oxford, Keble Road, Oxford OX13RH, United Kingdom*
[64]*University of Science and Technology Liaoning, Anshan 114051, People's Republic of China*
[65]*University of Science and Technology of China, Hefei 230026, People's Republic of China*
[66]*University of South China, Hengyang 421001, People's Republic of China*
[67]*University of the Punjab, Lahore-54590, Pakistan*
[68a]*University of Turin and INFN, University of Turin, I-10125 Turin, Italy*
[68b]*University of Eastern Piedmont, I-15121 Alessandria, Italy*
[68c]*INFN, I-10125 Turin, Italy*
[69]*Uppsala University, Box 516, SE-75120 Uppsala, Sweden*
[70]*Wuhan University, Wuhan 430072, People's Republic of China*
[71]*Xinyang Normal University, Xinyang 464000, People's Republic of China*
[72]*Yunnan University, Kunming 650500, People's Republic of China*
[73]*Zhejiang University, Hangzhou 310027, People's Republic of China*
[74]*Zhengzhou University, Zhengzhou 450001, People's Republic of China*

By analyzing an electron-positron collision data sample corresponding to an integrated luminosity of 2.93 fb^{-1} taken at the center-of-mass energy of 3.773 GeV with the BESIII detector, we obtain for the first

[a]Also at the Moscow Institute of Physics and Technology, Moscow 141700, Russia.
[b]Also at the Novosibirsk State University, Novosibirsk 630090, Russia.
[c]Also at the NRC "Kurchatov Institute", PNPI, 188300 Gatchina, Russia.
[d]Also at Goethe University Frankfurt, 60323 Frankfurt am Main, Germany.
[e]Also at Key Laboratory for Particle Physics, Astrophysics and Cosmology, Ministry of Education, Shanghai Key Laboratory for Particle Physics and Cosmology, Institute of Nuclear and Particle Physics, Shanghai 200240, People's Republic of China.
[f]Also at Key Laboratory of Nuclear Physics and Ion-beam Application (MOE) and Institute of Modern Physics, Fudan University, Shanghai 200443, People's Republic of China.
[g]Also at State Key Laboratory of Nuclear Physics and Technology, Peking University, Beijing 100871, People's Republic of China.
[h]Also at School of Physics and Electronics, Hunan University, Changsha 410082, People's Republic of China.
[i]Also at Guangdong Provincial Key Laboratory of Nuclear Science, Institute of Quantum Matter, South China Normal University, Guangzhou 510006, People's Republic of China.
[j]Also at Frontiers Science Center for Rare Isotopes, Lanzhou University, Lanzhou 730000, People's Republic of China.
[k]Also at Lanzhou Center for Theoretical Physics, Lanzhou University, Lanzhou 730000, People's Republic of China.
[l]Also at the Department of Mathematical Sciences, IBA, Karachi 75270, Pakistan.

time the absolute branching fractions for seven D^0 and D^+ hadronic decay modes and search for the hadronic decay $D^0 \to K_S^0 K_S^0 \pi^0$ with much improved sensitivity. The results are $\mathcal{B}(D^0 \to K_S^0 \pi^0 \pi^0 \pi^0) = (7.64 \pm 0.30 \pm 0.29) \times 10^{-3}$, $\mathcal{B}(D^0 \to K^- \pi^+ \pi^0 \pi^0 \pi^0) = (9.54 \pm 0.30 \pm 0.31) \times 10^{-3}$, $\mathcal{B}(D^0 \to K_S^0 \pi^+ \pi^- \pi^0 \pi^0) = (12.66 \pm 0.45 \pm 0.43) \times 10^{-3}$, $\mathcal{B}(D^+ \to K_S^0 \pi^+ \pi^0 \pi^0) = (29.04 \pm 0.62 \pm 0.87) \times 10^{-3}$, $\mathcal{B}(D^+ \to K_S^0 \pi^+ \pi^+ \pi^- \pi^0) = (15.28 \pm 0.57 \pm 0.60) \times 10^{-3}$, $\mathcal{B}(D^+ \to K_S^0 \pi^+ \pi^0 \pi^0 \pi^0) = (5.54 \pm 0.44 \pm 0.32) \times 10^{-3}$, $\mathcal{B}(D^+ \to K^- \pi^+ \pi^+ \pi^0 \pi^0) = (4.95 \pm 0.26 \pm 0.19) \times 10^{-3}$, and $\mathcal{B}(D^0 \to K_S^0 K_S^0 \pi^0) < 1.45 \times 10^{-4}$ at the 90% confidence level. Here, the first uncertainties are statistical, and the second ones are systematic. The newly studied decays greatly enrich the knowledge of the $D \to \bar{K}\pi\pi$ and $D \to \bar{K}\pi\pi\pi$ hadronic decays and open a bridge to access more two-body hadronic D decays containing scalar, vector, axial, and tensor mesons in the charm sector.

I. INTRODUCTION

Experimental investigations of hadronic D decays can greatly aid our understanding of strong and weak interactions [1–3]. For example, studies of hadronic D decays provide a way to explore the effects of $D^0 - \bar{D}^0$ mixing and charge-parity (CP) violation, which are key to understanding the asymmetry between matter and antimatter in the Universe [4]. In addition, the improved knowledge of the strong phase difference in various hadronic decays of neutral D mesons provides key information needed to extract the Cabibbo-Kobayashi-Maskawa (CKM) triangle angle of γ in B physics, which is crucial to test CKM matrix unitarity. In addition, amplitude analyses of multibody hadronic D decays help to access quasi-two-body hadronic D decays and to extract chiral structures of weak interaction in analogy to the multibody decay processes explored in Refs. [5,6]. Moreover, combining amplitude analysis results with the precisely measured branching fractions of these same hadronic D decays yields the branching fractions of two-body hadronic D decays, which are important to explore the phenomenon of quark SU(3)-flavor symmetry breaking [7–11].

Since the discovery of D mesons in the 1970s, hadronic D decays have been investigated extensively and precisely [12]. However, some multibody Cabibbo-favored decays, e.g., $D^0 \to K_S^0 \pi^0 \pi^0 \pi^0$, $K^- \pi^+ \pi^0 \pi^0 \pi^0$, $K_S^0 \pi^+ \pi^- \pi^0 \pi^0$, $D^+ \to K_S^0 \pi^+ \pi^0 \pi^0$, $K_S^0 \pi^+ \pi^0 \pi^0 \pi^0$, $K^- \pi^+ \pi^+ \pi^0 \pi^0$, and $K_S^0 \pi^+ \pi^+ \pi^- \pi^0$, remain unmeasured. Experimental studies of these decays are challenging mainly due to high background, low efficiency, and poor resolution. In this paper, we report on the measurements of the absolute branching fractions for these multibody decays by analyzing the e^+e^- collision data sample corresponding to an integrated luminosity of 2.93 fb^{-1} [13,14] collected at the center-of-mass energy of $\sqrt{s} = 3.773$ GeV with the BESIII detector. Throughout this paper, charge conjugate processes are always implied.

II. BESIII DETECTOR AND MONTE CARLO SIMULATION

The BESIII detector is a magnetic spectrometer [15] located at the Beijing Electron Positron Collider (BEPCII) [16]. The cylindrical core of the BESIII detector consists of a helium-based multilayer drift chamber (MDC), a plastic scintillator time-of-flight system (TOF), and a CsI (Tl) (TI doped CsI crystal) electromagnetic calorimeter (EMC), which are all enclosed in a superconducting solenoidal magnet providing a 1.0 T magnetic field. The solenoid is supported by an octagonal flux-return yoke with resistive-plate counter muon-identifier modules interleaved with steel. The acceptance of charged particles and photons is 93% over a 4π solid angle. The charged-particle momentum resolution at 1 GeV/c is 0.5%, and the resolution of the specific ionization energy loss (dE/dx) is 6% for the electrons from Bhabha scattering. The EMC measures photon energies with a resolution of 2.5% (5%) at 1 GeV in the barrel (end cap) region. The time resolution of the TOF barrel part is 68 ps, while that of the end cap part is 110 ps.

Simulated samples, produced with the GEANT4-based [17] Monte Carlo (MC) package including the geometric description of the BESIII detector and the detector response, are used to determine the detection efficiency and to estimate the backgrounds. The simulation includes the beam-energy spread and initial-state radiation in the e^+e^- annihilations modeled with the generator KKMC [18]. The inclusive MC samples consist of the production of $D\bar{D}$ pairs, the non-$D\bar{D}$ decays of the $\psi(3770)$, the initial-state radiation production of the J/ψ and $\psi(3686)$ states, and the continuum processes. The known decay modes are modeled with EVTGEN [19] using the branching fractions taken from the Particle Data Group (PDG) [12], and the remaining unknown decays from the charmonium states are modeled with LUNDCHARM [20,21]. The final-state radiation from charged final-state particles is incorporated with the PHOTOS package [22].

III. MEASUREMENT METHOD

The $D^0 \bar{D}^0$ or $D^+ D^-$ pairs are produced without any additional hadron in e^+e^- annihilations at $\sqrt{s} = 3.773$ GeV. This process offers a clean environment to measure the branching fractions of hadronic D decays with the double-tag method [23]. The single-tag candidate events are

selected by reconstructing a $\bar{D}^0$ or D^- in the following hadronic final states: $\bar{D}^0 \to K^+\pi^-$, $K^+\pi^-\pi^0$, $K^+\pi^-\pi^-\pi^+$, and $D^- \to K^+\pi^-\pi^-$, $K_S^0\pi^-$, $K^+\pi^-\pi^-\pi^0$, $K_S^0\pi^-\pi^0$, $K_S^0\pi^+\pi^-\pi^-$, $K^+K^-\pi^-$. The event in which a signal candidate is selected in the presence of a single-tag (ST) $\bar{D}$ meson is called a double-tag (DT) event. The branching fraction for the signal decay is determined by

$$\mathcal{B}_{\text{sig}} = N_{\text{DT}}^{\text{net}}/(N_{\text{ST}}^{\text{tot}} \cdot \epsilon_{\text{sig}}), \tag{1}$$

where $N_{\text{ST}}^{\text{tot}} = \sum_i N_{\text{ST}}^i$ and $N_{\text{DT}}^{\text{net}}$ are the total single-tag yield and signal yield in data, respectively, in which N_{ST}^i is the single-tag yield for the tag mode i. For the signal decays involving K_S^0 meson(s) in the final states, $N_{\text{DT}}^{\text{net}}$ is the net signal yield after removing the peaking background, which is dominated by the corresponding non-K_S^0 decays. The yield of the peaking background is also obtained from the fit with the double-tag method. For the other signal decays, the variable only corresponds to the fitted double-tag yields. Further details are described in Sec. VI. Here, ϵ_{sig} is the efficiency of detecting the signal D decay, averaged over all tag modes i, which is given by

$$\epsilon_{\text{sig}} = \sum_i (N_{\text{ST}}^i \cdot \epsilon_{\text{DT}}^i/\epsilon_{\text{ST}}^i)/N_{\text{ST}}^{\text{tot}}, \tag{2}$$

where ϵ_{ST}^i and ϵ_{DT}^i are the efficiencies of detecting single-tag and double-tag candidates in the tag mode i, respectively.

The measurements of the branching fractions of neutral, self-conjugate D decays have to be corrected for the effects of quantum correlation (QC) existing in the data but not being implemented in the MC simulation. For each neutral D decay, the CP-even component is estimated by the CP-even tag $D^0 \to K^+K^-$ and the CP-odd tag $D^0 \to K_S^0\pi^0$. Using the same method as described in Ref. [24] and the parameters quoted from Refs. [25–27], we find the correction factors (f_{QC}) that account for the QC effect on the measured branching fractions to be $1.081 \pm 0.007_{\text{stat}}$ and $0.956 \pm 0.006_{\text{stat}}$ for $D^0 \to K_S^0\pi^0\pi^0\pi^0$ and $D^0 \to K_S^0\pi^+\pi^-\pi^0\pi^0$, respectively. Here, f_{QC} multiplies the naively extracted branching fractions.

IV. EVENT SELECTION

The selection criteria of $K^\pm$, $\pi^\pm$, K_S^0, and π^0 are the same as those used in the analyses presented in Refs. [28–30]. All charged tracks, except those originating from K_S^0 decays, are required to have a polar angle θ with respect to the beam direction within the MDC acceptance $|\cos\theta| < 0.93$ and a distance of closest approach to the interaction point within 10 cm along the beam direction and within 1 cm in the plane perpendicular to the beam direction. Particle identification (PID) for charged pions and kaons is performed by exploiting TOF information and the dE/dx measured by the MDC. The confidence levels for pion and kaon hypotheses (CL_π and CL_K) are calculated. Kaon and pion candidates are required to satisfy $CL_K > CL_\pi$ and $CL_\pi > CL_K$, respectively.

The K_S^0 candidates are reconstructed from two oppositely charged tracks which are assigned as pions with no PID criteria applied. These charged tracks must satisfy $|\cos\theta| < 0.93$. In addition, due to the long lifetime of the K_S^0 meson, there is a less stringent criterion on the distance of closest approach to the interaction point in the beam direction of less than 20 cm and no requirement on the distance of closest approach in the plane transverse to the beam direction. Furthermore, the $\pi^+\pi^-$ pairs are constrained to originate from a common vertex, and their invariant mass is required to be within $(0.486, 0.510)$ GeV/c^2, which corresponds to about three times the fitted resolution around the K_S^0 nominal mass. The decay length of the K_S^0 candidate is required to be greater than two standard deviations of the vertex resolution away from the interaction point.

The π^0 candidate is reconstructed via its $\gamma\gamma$ decay. The photon candidates are selected using the information from the EMC showers. It is required that each EMC shower starts within 700 ns of the event start time and its energy is greater than 25 (50) MeV in the barrel (end cap) region of the EMC [15]. The energy deposited in the neighboring TOF counters is included to improve the reconstruction efficiency and energy resolution as the correctness of the shower energy. The opening angle between the candidate shower and the nearest charged track must be greater than 10°. The $\gamma\gamma$ pair is taken as a π^0 candidate if its invariant mass is within $(0.115, 0.150)$ GeV/c^2. To improve the resolution, a kinematic fit constraining the $\gamma\gamma$ invariant mass to the π^0 nominal mass [12] is imposed on the selected photon pair.

V. YIELDS OF SINGLE-TAG $\bar{D}$ MESONS

To select $\bar{D}^0 \to K^+\pi^-$ candidates, the backgrounds from cosmic rays and Bhabha events are rejected by using the same requirements described in Ref. [31]. In the selection of $\bar{D}^0 \to K^+\pi^-\pi^-\pi^+$ candidates, the $\bar{D}^0 \to K_S^0K^\pm\pi^\mp$ decays are suppressed by requiring the mass of all $\pi^+\pi^-$ pairs to be outside $(0.483, 0.513)$ GeV/c^2.

The tagged $\bar{D}$ mesons are identified using two variables, namely, the energy difference

$$\Delta E_{\text{tag}} \equiv E_{\text{tag}} - E_{\text{b}}, \tag{3}$$

and the beam-constrained mass

$$M_{\text{BC}}^{\text{tag}} \equiv \sqrt{E_{\text{b}}^2 - |\vec{p}_{\text{tag}}|^2}. \tag{4}$$

Here, E_{b} is the beam energy, and $\vec{p}_{\text{tag}}$ and E_{tag} are the momentum and energy of the $\bar{D}$ candidate in the rest frame of e^+e^- system, respectively. For each tag mode, if there are multiple candidates (about 10% of the selected events)
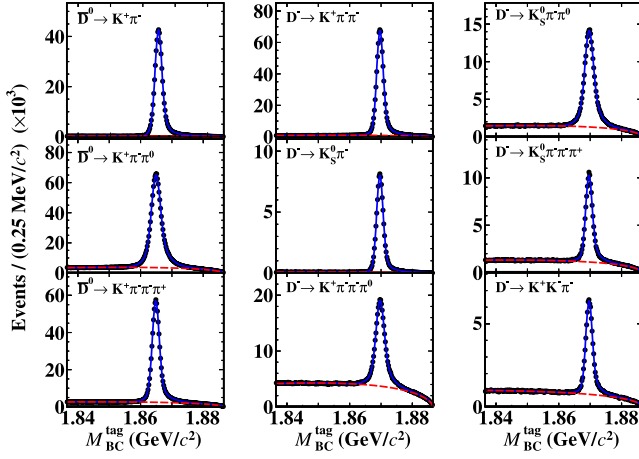
FIG. 1. Fits to the $M_{\rm BC}$ distributions of the single-tag $\bar{D}^0$ (left column) and D^- (middle and right columns) candidates, where the points with error bars are data and the blue solid and red dashed curves are the fit results and the fitted backgrounds, respectively.

in an event, only the one with the least $|\Delta E_{\rm tag}|$ is kept. The tagged $\bar{D}$ candidates are required to satisfy $\Delta E_{\rm tag} \in (-55, 40)$ MeV for the tag modes containing π^0 in the final states and $\Delta E_{\rm tag} \in (-25, 25)$ MeV for the other tag modes, due to differing resolutions.

To extract the yields of single-tag $\bar{D}$ mesons for individual tag modes, binned maximum-likelihood fits are performed on the $M_{\rm BC}^{\rm tag}$ distributions of the single-tag candidates, following Refs. [28–30]. In the fits, the $\bar{D}$ signal is modeled by an MC-simulated shape convolved with a double-Gaussian function describing the resolution difference between data and MC simulation. The combinatorial background shape is described by an ARGUS function [32] defined as $c_{M_{\rm BC}^{\rm tag}}(M_{\rm BC}^{\rm tag}; E_{\rm end}, \xi_{M_{\rm BC}^{\rm tag}}) = A_{M_{\rm BC}^{\rm tag}} \cdot M_{\rm BC}^{\rm tag} \cdot \sqrt{1 - \frac{M_{\rm BC}^{{\rm tag}\,2}}{E_{\rm end}^2/c^4}} \cdot \exp\left[\xi_{M_{\rm BC}^{\rm tag}}\left(1 - \frac{M_{\rm BC}^{{\rm tag}\,2}}{E_{\rm end}^2/c^4}\right)\right]$, where $E_{\rm end}$ is an end point fixed at 1.8865 GeV (corresponding to the beam energy), $A_{M_{\rm BC}^{\rm tag}}$ is a normalization factor, and

$\xi_{M_{\rm BC}^{\rm tag}}$ is a free parameter. The resulting fits to the $M_{\rm BC}$ distributions for various tag modes are shown in Fig. 1. The total yields of the single-tag $\bar{D}^0$ and D^- mesons in data are $(232.8 \pm 0.2) \times 10^4$ and $(155.8 \pm 0.2) \times 10^4$, respectively, where the uncertainties are statistical only.

VI. YIELDS OF DOUBLE-TAG EVENTS

The signal D decays are selected by using the remaining tracks and showers that have not been used to reconstruct the single-tag $\bar{D}$ candidates. Charged D signal candidates must have charge opposite to the tag; for neutral D, signal candidates must have oppositely charged kaons in the cases where both kaons are charged. For $D^0 \to K_S^0 \pi^+ \pi^- \pi^0 \pi^0$ and $D^+ \to K_S^0 \pi^+ \pi^+ \pi^- \pi^0$, to suppress backgrounds from $D^0 \to K_S^0 K_S^0(\to \pi^+\pi^-)\pi^0\pi^0$ and $D^+ \to K_S^0 K_S^0(\to \pi^+\pi^-)\pi^+\pi^0$ decays, the $\pi^+\pi^-$ invariant masses are required to be outside $(0.468, 0.528)$ GeV/c^2. The signal decays that have two or more π^0s can have background contamination from a corresponding decay where the $\pi^0\pi^0$ pair originates from a K_S^0 meson. The rate of these backgrounds is typically small and is estimated with the known branching fractions taken from the PDG [12] except for the background of $D^0 \to K_S^0 K_S^0(\to \pi^0\pi^0)\pi^0$ for $D^0 \to K_S^0\pi^0\pi^0\pi^0$. The upper limit on the branching fraction of $D^0 \to K_S^0 K_S^0 \pi^0$ is reestimated via $K_S^0(\to \pi^+\pi^-)K_S^0(\to\pi^+\pi^-)\pi^0$. The data obtained at BESIII allow for a more accurate estimate than the current PDG limit [12]. Since these peaking backgrounds are small, a veto is not applied on $M_{\pi^0\pi^0}$ due to a significant reduction of the signal efficiency. The expected yields of these peaking backgrounds are fixed in our fit to $M_{\rm BC}^{\rm tag}$ versus $M_{\rm BC}^{\rm sig}$.

The signal D mesons are identified using the energy difference $\Delta E_{\rm sig}$ and the beam-constrained mass $M_{\rm BC}^{\rm sig}$, which are calculated with the "sig" analogs of the "tag" equations (3) and (4). For each signal mode, if there are multiple candidates in an event, only the one with the

TABLE I. Requirements of $\Delta E_{\rm sig}$, the fitted and net yields of double-tag candidates ($N_{\rm DT}^{\rm fit}$ and $N_{\rm DT}^{\rm net}$), background yield in the K_S^0 sideband ($N_{K_S^0,{\rm sid}}$), signal efficiencies ($\epsilon_{\rm sig}$), and the obtained branching fractions ($\mathcal{B}_{\rm sig}$) for various signal decays. The first and second uncertainties for $\mathcal{B}_{\rm sig}$ are statistical and systematic, respectively, while the uncertainties for $N_{\rm DT}^{\rm fit}$, $N_{K_S^0,{\rm sid}}$, $N_{\rm DT}^{\rm net}$, and $\epsilon_{\rm sig}$ are statistical only. For $D^0 \to K_S^0 K_S^0 \pi^0$, the $N_{\rm DT}^{\rm net}$ and $\mathcal{B}_{\rm sig}$ are set at 90% confidence level. The $N_{K_S^0,{\rm sid}}$ denotes the net K_S^0 background yield combined sideband 1 and sideband 2 regions.

Signal mode	$\Delta E_{\rm sig}$ (MeV)	$N_{\rm DT}^{\rm fit}$	$N_{K_S^0,{\rm sid}}$	$N_{\rm DT}^{\rm net}$	$\epsilon_{\rm sig}$ (%)	$\mathcal{B}_{\rm sig}$ (10^{-3})
$D^0 \to K_S^0\pi^0\pi^0\pi^0$	$(-73, 34)$	913 ± 33	86 ± 11	870 ± 36	4.90 ± 0.04	$7.64 \pm 0.30 \pm 0.29$
$D^0 \to K^-\pi^+\pi^0\pi^0\pi^0$	$(-64, 33)$	1560 ± 48	$\cdots$	1560 ± 48	7.04 ± 0.06	$9.54 \pm 0.30 \pm 0.31$
$D^0 \to K_S^0\pi^+\pi^-\pi^0\pi^0$	$(-50, 30)$	1253 ± 40	134 ± 14	1186 ± 40	4.04 ± 0.04	$12.66 \pm 0.45 \pm 0.43$
$D^+ \to K_S^0\pi^+\pi^0\pi^0$	$(-63, 34)$	3513 ± 66	226 ± 19	3400 ± 66	7.51 ± 0.07	$29.04 \pm 0.62 \pm 0.87$
$D^+ \to K_S^0\pi^+\pi^+\pi^-\pi^0$	$(-45, 30)$	1097 ± 37	107 ± 14	1043 ± 38	4.38 ± 0.04	$15.28 \pm 0.57 \pm 0.60$
$D^+ \to K_S^0\pi^+\pi^0\pi^0\pi^0$	$(-43, 25)$	294 ± 22	19 ± 7	285 ± 23	3.30 ± 0.03	$5.54 \pm 0.44 \pm 0.32$
$D^+ \to K^-\pi^+\pi^+\pi^0\pi^0$	$(-54, 31)$	756 ± 39	$\cdots$	756 ± 39	9.80 ± 0.07	$4.95 \pm 0.26 \pm 0.19$
$D^0 \to K_S^0 K_S^0\pi^0$	$(-45, 28)$	65 ± 10	118 ± 13	$6 \pm 13(<24.6)$	7.06 ± 0.11	<0.145
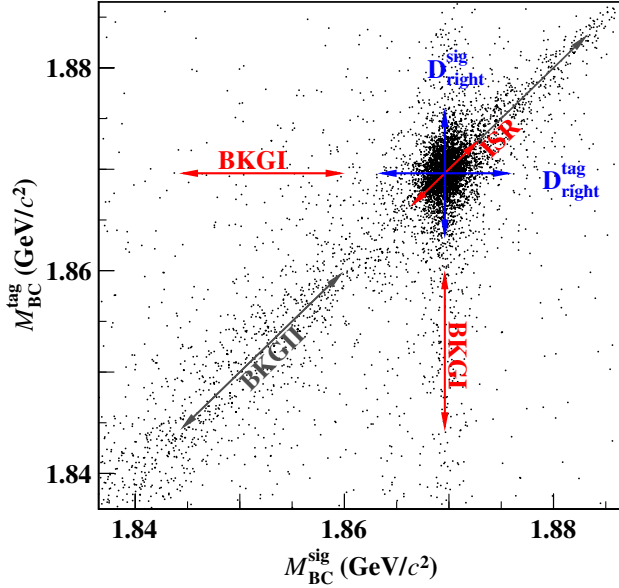
FIG. 2. Distribution of $M_{\mathrm{BC}}^{\mathrm{tag}}$ versus $M_{\mathrm{BC}}^{\mathrm{sig}}$ of the accepted candidates for $D^+ \to K_S^0 \pi^+ \pi^0 \pi^0$ versus all D^- tag modes in data. Here, ISR denotes the signal spreading along the diagonal direction. The $D_{\mathrm{right}}^{\mathrm{sig}}$ and $D_{\mathrm{right}}^{\mathrm{tag}}$ denotes the signal spreading around $M_{\mathrm{BC}}^{\mathrm{sig}} = M_D$ and $M_{\mathrm{BC}}^{\mathrm{tag}} = M_D$.

smallest $|\Delta E_{\mathrm{sig}}|$ is kept. The signal decays are required to satisfy the mode-dependent ΔE_{sig} requirements, as shown in the second column of Table I.

Figure 2 shows the $M_{\mathrm{BC}}^{\mathrm{tag}}$ versus $M_{\mathrm{BC}}^{\mathrm{sig}}$ distribution of the accepted double-tag candidates in data. The signal events concentrate around $M_{\mathrm{BC}}^{\mathrm{tag}} = M_{\mathrm{BC}}^{\mathrm{sig}} = M_D$, where M_D is the D nominal mass [12]. The events with correctly reconstructed D ($\bar{D}$) and incorrectly reconstructed $\bar{D}$ (D), defined as BKGI, are spread along the lines around $M_{\mathrm{BC}}^{\mathrm{tag}} = M_D$ or $M_{\mathrm{BC}}^{\mathrm{sig}} = M_D$. The events smeared along the diagonal, defined as BKGII, are mainly from the $e^+ e^- \to q\bar{q}$ processes and incorrectly reconstructed $D\bar{D}$. The events with uncorrelated and incorrectly reconstructed D and $\bar{D}$, defined as BKGIII, disperse in the whole allowed kinematic region.

For each signal D decay mode, the yield of double-tag events ($N_{\mathrm{DT}}^{\mathrm{fit}}$) is obtained from a two-dimensional (2D) binned maximum-likelihood fit [33] on the $M_{\mathrm{BC}}^{\mathrm{tag}}$ versus $M_{\mathrm{BC}}^{\mathrm{sig}}$ distribution of the accepted candidates. In the fit, the probability density functions (PDFs) of signal, BKGI, BKGII, and BKGIII are constructed as:

   (i) signal: $a(x, y)$,
   (ii) BKGI: $b(x) \cdot c_y(y; E_{\mathrm{b}}, \xi_y) + b(y) \cdot c_x(x; E_{\mathrm{b}}, \xi_x)$,
   (iii) BKGII: $c_z(z; \sqrt{2}E_{\mathrm{b}}, \xi_z) \cdot g(k)$, and
   (iv) BKGIII: $c_x(x; E_{\mathrm{b}}, \xi_x) \cdot c_y(y; E_{\mathrm{b}}, \xi_y)$,

respectively. Here, $x = M_{\mathrm{BC}}^{\mathrm{sig}}$, $y = M_{\mathrm{BC}}^{\mathrm{tag}}$, $z = (x + y)/\sqrt{2}$, and $k = (x - y)/\sqrt{2}$. The PDFs of signals $a(x, y)$, $b(x)$, and $b(y)$ are described by the corresponding MC-simulated
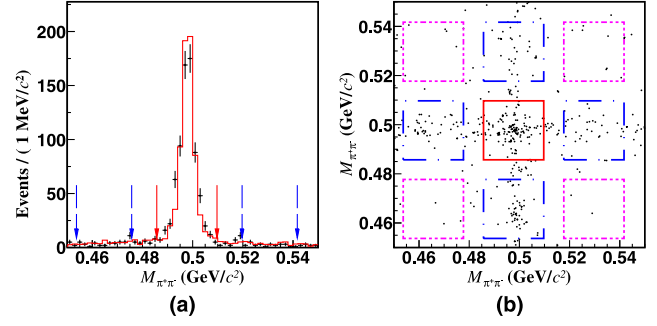

FIG. 3. (a) $\pi^+\pi^-$ invariant-mass distributions of the $D^0 \to K_S^0 \pi^0 \pi^0 \pi^0$ candidate events of data (points with error bars) and inclusive MC sample (histogram). Pairs of the red solid (blue dashed) arrows denote the K_S^0 signal (sideband) regions. (b) Distribution of $M_{\pi^+\pi^-(1)}$ versus $M_{\pi^+\pi^-(2)}$ for the $D^0 \to K_S^0 K_S^0 \pi^0$ candidate events in data. The red solid box denotes the 2D signal region. Blue dashed (pink dot-dashed) boxes indicate the 2D sideband 1 (2) regions.

shapes, and $c_f(f; E_{\mathrm{end}}, \xi_f)$ is an ARGUS function [32] defined above, where f denotes x, y, or z; E_{b} is fixed at 1.8865 GeV. The signal shape $a(x, y)$ is also convolved with a 2D Gaussian function. The PDF $g(k)$ is a Gaussian function with mean of zero and standard deviation parametrized by $\sigma_k = \sigma_0 \cdot (\sqrt{2}E_{\mathrm{b}}/c^2 - k)^p$, where σ_0 and p are fit parameters.

The signal decays with one $K_S^0 (\to \pi^+\pi^-)$ have background contamination from corresponding decays which have combinatorial $\pi^+\pi^-$ pairs that satisfy the K_S^0 selection criteria. They form peaking backgrounds around M_D in the $M_{\mathrm{BC}}^{\mathrm{sig}}$ distributions. This kind of peaking background is estimated by selecting events in the one-dimensional (1D) K_S^0 sideband region of $(0.454, 0.478) \cup (0.518, 0.542)$ GeV/c^2.

Since there are two K_S^0 mesons in $D^0 \to K_S^0 K_S^0 \pi^0$, 2D signal and sideband regions are used. The 2D K_S^0 signal region is defined as the square region with both $\pi^+\pi^-$ combinations lying in the K_S^0 signal regions. The 2D K_S^0 sideband 1 regions are defined as the square regions with one $\pi^+\pi^-$ combination located in the 1D K_S^0 sideband regions and the other in the 1D K_S^0 signal region. The sideband 2 regions are defined as the square regions with both $\pi^+\pi^-$ combinations located in the 1D K_S^0 sideband regions. Figure 3 shows 1D and 2D $\pi^+\pi^-$ invariant-mass distributions as well as the K_S^0 signal and sideband regions.

For the signal decays involving K_S^0 meson(s) in the final states, the net yields of DT events are calculated by subtracting the sideband contribution from the DT fitted yield by

$$N_{\mathrm{DT}}^{\mathrm{net}} = N_{\mathrm{DT}}^{\mathrm{fit}} + \sum_i^N \left[\left(-\frac{1}{2}\right)^i N_{\mathrm{sid}i}^{\mathrm{fit}} \right], \qquad (5)$$

where $N_{\mathrm{DT}}^{\mathrm{fit}}$ and $N_{\mathrm{sid}i}^{\mathrm{fit}}$ are the fitted D yields in the 1D or 2D signal region and sideband i region, respectively, where i runs from 1. This relation has been verified by a large MC
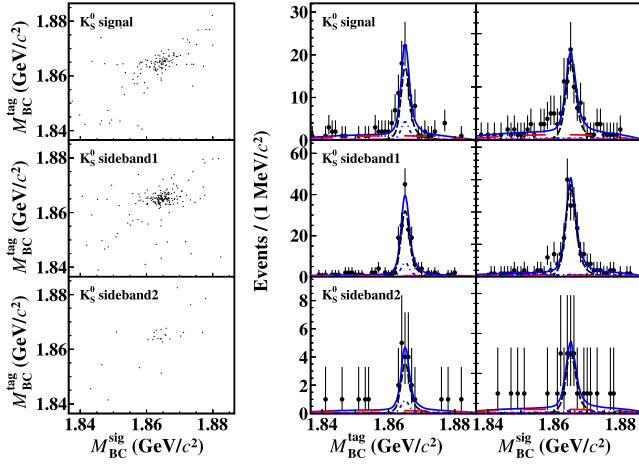
FIG. 4. Scatter plots (left) and projections of M_{BC}^{tag} and M_{BC}^{sig} (right) for the 2D fits on the candidate events for $D^0 \to K_S^0 K_S^0 \pi^0$. In the projections, the dots with error bars are data, and the blue solid curves are the total fit results. The black dotted curves are the fitted signal, the blue dot-dashed curves are the BKGI, the red dot-long-dashed curves are the BKGII, and the pink long-dashed curves are the BKGIII.

sample. Here, $N = 1$ for the decays with one K_S^0 meson, while $N = 2$ for the decays with two K_S^0 mesons. The combinatorial $\pi^+\pi^-$ backgrounds are assumed to be uniformly distributed, and double-counting is avoided by subtracting sideband 2 yields from sideband 1 yields appropriately. For the other signal decays, the net yields of double-tag events are N_{DT}^{fit}.

To obtain a more reliable peaking background yield from $D^0 \to K_S^0(\to \pi^+\pi^-) K_S^0(\to \pi^0\pi^0)\pi^0$ in the study of $D^0 \to K_S^0 \pi^0 \pi^0 \pi^0$, we have reestimated the branching
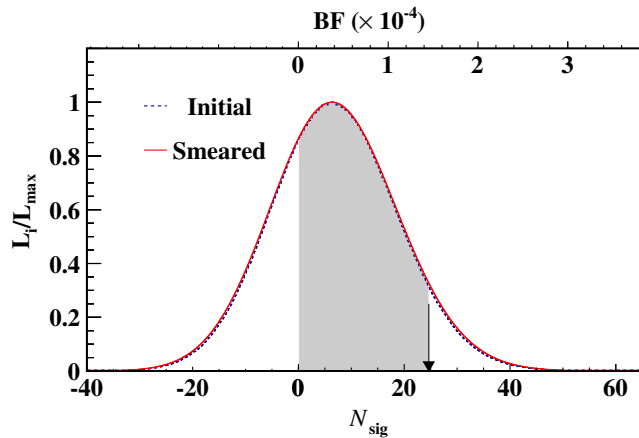
FIG. 5. Distribution of likelihood versus the assumed signal yield or branching fraction for $D^0 \to K_S^0 K_S^0 \pi^0$. Here, L_{max} denotes the maximum likelihood obtained from the fit. The results obtained with and without incorporating the systematic uncertainties are shown as the red solid and black dashed curves, respectively. The black arrow shows the result corresponding to the 90% confidence level.

fraction of $D^0 \to K_S^0 K_S^0 \pi^0$ via $K_S^0(\to \pi^+\pi^-) K_S^0(\to \pi^+\pi^-)\pi^0$. Simultaneous two-dimensional maximum-likelihood fits are performed on the candidates for $D^0 \to K_S^0(\to \pi^+\pi^-)\times K_S^0(\to \pi^+\pi^-)\pi^0$ in the 2D K_S^0 signal, sideband 1, and sideband 2 regions, as shown in Fig. 4.

In the fits, the background yields in the 2D K_S^0 sideband 1 and sideband 2 regions have been subtracted using Eq. (5). No significant signal of $D^0 \to K_S^0 K_S^0 \pi^0$ is found. The resulting upper limit on the branching fraction for $D^0 \to K_S^0 K_S^0 \pi^0$ is 1.57×10^{-4} at a 90% confidence level, using the Bayesian approach [34] after incorporating the systematic uncertainty discussed in Sec. VII. The distribution of likelihood versus branching fraction is shown in Fig. 5.

Figure 6 shows the M_{BC}^{tag} and M_{BC}^{sig} projections of the 2D fits to data. For the candidate events in the 2D K_S^0 sideband region, the 2D fits are performed similarly. From these fits,
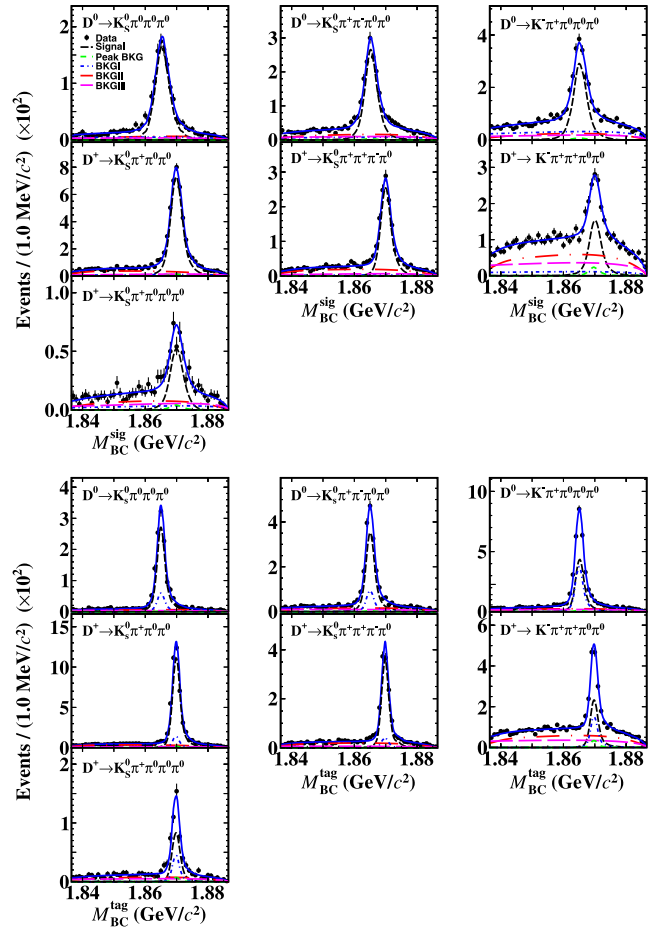

FIG. 6. Projections of M_{BC}^{tag} and M_{BC}^{sig} distributions for the 2D fits to the double-tag candidate events with all $\bar{D}^0$ or D^- tags. Data are shown as points with error bars. Blue solid, black dotted, blue dot-dashed, red dot-long-dashed, pink long-dashed, and green dashed curves denote the overall fit results, signal, BKGI, BKGII, BKGIII, and peaking background components (see the text), respectively.
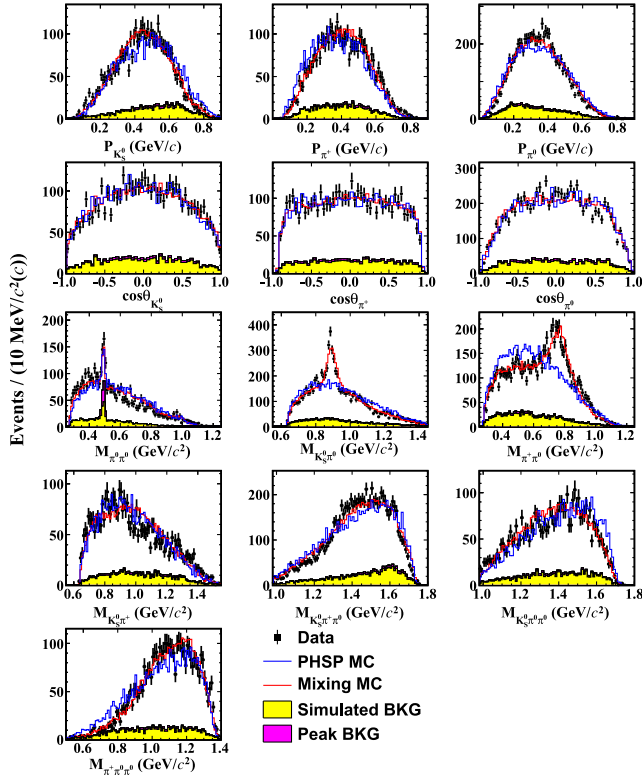
FIG. 7. Comparisons of some typical distributions for the $D^+ \to K_S^0 \pi^+ \pi^0 \pi^0$ candidate events between data (dots with error bars) and the signal MC events (blue dotted/red dashed histograms) plus the MC-simulated backgrounds from the inclusive MC sample (yellow histograms).

we obtain the DT yields for the individual signal decays as shown in Table I.

The double-tag efficiencies are determined from an MC simulation. To account for the effect of intermediate resonance structure on the efficiency, each of these decays is modeled by the corresponding mixed-signal MC samples, in which the dominant decay modes containing resonances of η, ω, $K^*(892)$, $\rho(770)$, $f_0(980)$, $K_1(1270)$, and $K_1(1400)$ are mixed with the phase-space (PHSP) signal MC samples. The mixing ratios are determined by examining the corresponding invariant mass and momentum spectra. The momentum and the polar angle distributions of the daughter particles and the invariant masses of each two-, three-, and four-body particle combinations of the data agree with those of the MC simulations. As an example, Fig. 7 shows the momentum and the polar angle distributions of the daughter particles, the invariant mass distributions of two- or three-body particle combinations of the candidates for $D^+ \to K_S^0 \pi^+ \pi^0 \pi^0$ between data and MC simulations.

The measured values of $N_{\mathrm{DT}}^{\mathrm{net}}$, ϵ_{sig}, and the obtained branching fractions are summarized in Table I. The signal efficiencies have been corrected by the data-MC differences in the selection efficiencies of $K^\pm$ and $\pi^\pm$ tracking and PID

procedures and π^0 reconstruction. These efficiencies also include the branching fractions of the K_S^0 and π^0 decays.

VII. SYSTEMATIC UNCERTAINTIES

The systematic uncertainties are estimated relative to the measured branching fractions and are discussed below. In the determination of the branching fractions using Eq. (1), all uncertainties associated with the selection of tagged $\bar{D}$ are canceled. The systematic uncertainties in the total yields of single-tag $\bar{D}$ mesons, which are mainly due to the fits to the M_{BC} distributions of the single-tag $\bar{D}$ candidates, were previously estimated to be 0.5% for both neutral and charged $\bar{D}$ [28–30].

The tracking and PID efficiencies for $K^\pm$ or $\pi^\pm$, $\epsilon_{K\mathrm{or}\pi}^{\mathrm{tracking(PID)}}$[data], and $\epsilon_{K\mathrm{or}\pi}^{\mathrm{tracking(PID)}}$ [MC] are investigated using double-tag $D\bar{D}$ hadronic events. The averaged ratios between data and MC efficiencies ($f_{K\mathrm{or}\pi}^{\mathrm{tracking(PID)}} = \epsilon_{K\mathrm{or}\pi}^{\mathrm{tracking(PID)}}$[data]$/\epsilon_{K\mathrm{or}\pi}^{\mathrm{tracking(PID)}}$[MC]) of tracking (PID) for $K^\pm$ or $\pi^\pm$ are weighted by the corresponding momentum spectra of signal MC events, giving f_K^{tracking} ranging from 1.019–1.032 and $f_\pi^{\mathrm{tracking}}$ close to unity for all seven signal modes. After correcting the MC efficiencies by f_K^{tracking}, the statistical uncertainties of $f_{K\mathrm{or}\pi}^{\mathrm{tracking}}$ are assigned as the systematic uncertainties of tracking efficiencies, which are 0.2% per $K^\pm$ and (0.2–0.3)% per $\pi^\pm$. f_K^{PID} and f_π^{PID} are all close to unity and their individual uncertainties, (0.2–0.3)%, are taken as the associated systematic uncertainties per $K^\pm$ or $\pi^\pm$.

The systematic error related to the uncertainty in the K_S^0 reconstruction efficiency is estimated from measurements of $J/\psi \to K^*(892)^\mp K^\pm$ and $J/\psi \to \phi K_S^0 K^\pm \pi^\mp$ control samples [35] and found to be 1.6% per K_S^0. The systematic uncertainty of π^0 reconstruction efficiency is assigned as (0.7–0.8)% per π^0 from a study of double-tag $D\bar{D}$ hadronic decays of $\bar{D}^0 \to K^+ \pi^- \pi^0$ and $\bar{D}^0 \to K_S^0 \pi^0$ decays tagged by either $D^0 \to K^- \pi^+$ or $D^0 \to K^- \pi^+ \pi^+ \pi^-$ [28,29]. The systematic uncertainty in the 2D fit to the $M_{\mathrm{BC}}^{\mathrm{tag}}$ versus $M_{\mathrm{BC}}^{\mathrm{sig}}$ distribution is examined via the repeated measurements in which the signal shape ($\pm 1\sigma$ in mean and width of smearing Gaussian) and the end point of the ARGUS function (± 0.2 MeV/c^2) are varied. Quadratically summing the changes of the branching fractions for these two sources yields the corresponding systematic uncertainties of (0.8–4.9)%.

The systematic uncertainty due to the ΔE_{sig} requirement is assigned to be (0.3–0.8)% for various signal decays, which corresponds to the largest efficiency difference with and without smearing the data-MC Gaussian resolution of ΔE_{sig} for signal MC events. Here, the smeared Gaussian parameters are obtained by using the samples of double-tag events $D^0 \to K_S^0 \pi^0$, $D^0 \to K^- \pi^+ \pi^0$, $D^0 \to K^- \pi^+ \pi^0 \pi^0$, and $D^+ \to K^- \pi^+ \pi^+ \pi^0$ versus the same $\bar{D}$ tags in our nominal analysis. The systematic uncertainties due to K_S^0 sideband

TABLE II. Relative systematic uncertainties (%) in the branching fraction measurements of the signal decays (1) $D^0 \to K_S^0 \pi^0 \pi^0 \pi^0$, (2) $D^0 \to K^- \pi^+ \pi^0 \pi^0 \pi^0$, (3) $D^0 \to K_S^0 \pi^+ \pi^- \pi^0 \pi^0$, (4) $D^+ \to K_S^0 \pi^+ \pi^0 \pi^0$, (5) $D^+ \to K_S^0 \pi^+ \pi^+ \pi^- \pi^0$, (6) $D^+ \to K_S^0 \pi^+ \pi^0 \pi^0 \pi^0$, (7) $D^+ \to K^- \pi^+ \pi^+ \pi^0 \pi^0$, and (8) $D^0 \to K_S^0 K_S^0 \pi^0$. Uncertainties which are not applicable are denoted by "–".

Source	1	2	3	4	5	6	7	8
N_{ST}^{tot}	0.5	0.5	0.5	0.5	0.5	0.5	0.5	0.5
$(K/\pi)^\pm$ tracking	–	0.4	0.4	0.2	0.6	0.2	0.6	–
$(K/\pi)^\pm$ PID	–	0.4	0.4	0.2	0.6	0.2	0.6	–
K_S^0 reconstruction	1.6	1.6	–	1.6	1.6	1.6	–	3.2
π^0 reconstruction	2.1	2.1	1.4	1.4	0.7	2.1	1.4	0.7
2D fit	1.8	2.0	1.9	0.8	1.6	4.9	3.5	3.9
ΔE_{sig} requirement	0.3	0.6	0.5	0.7	0.4	0.8	0.6	0.6
Quoted $\mathcal{B}$	0.12	0.10	0.10	0.10	0.08	0.12	0.07	0.14
MC modeling	1.8	0.6	1.2	1.6	2.9	0.8	0.3	–
MC statistics	0.7	0.8	0.9	0.6	0.8	0.9	0.6	0.5
QC effect	0.7	0.6	0.6	–	–	–	–	0.7
Total	3.8	3.3	3.4	3.0	4.0	5.8	4.0	5.2

choice and K_S^0 rejection mass window are cross-checked by examining the changes of the branching fractions via varying nominal K_S^0 sideband and corresponding rejection window by ± 5 MeV/c^2. The shifts in the fitted results are negligible in the cross-check, and hence no further systematic uncertainty is considered. For the decays whose efficiencies are estimated with mixed signal MC events, the imperfect simulations of the momentum and $\cos\theta$ distributions of charged particles are considered as a source of systematic uncertainty listed as the MC modeling. To estimate this systematic uncertainty, we examine the change of the signal efficiency after removing the most significant mixed component except for the processes containing η and ω. In addition, for the decays involving $D \to \bar{K}\pi\eta$ and $D \to \bar{K}\pi\omega$, we vary the known branching fractions of $D \to \bar{K}\pi\eta$ and $D \to \bar{K}\pi\omega$ by $\pm 1\sigma$. For each signal decay, the quadratic sum of the efficiency changes is assigned as the corresponding systematic uncertainty. The change of the reweighted to nominal efficiencies, (0.3–2.9)% for various signal decays, is assigned as the corresponding systematic uncertainty.

For $D^0 \to K_S^0 \pi^0 \pi^0 \pi^0$ and $D^0 \to K_S^0 \pi^+ \pi^- \pi^0 \pi^0$, after correcting the measured branching fractions by the QC factors, the residual uncertainties, 0.7% and 0.6%, are assigned as

individual systematic uncertainties. The QC effect on $D^0 \to K^- \pi^+ \pi^0 \pi^0 \pi^0$ appearing through mixing and doubly-Cabibbo-suppressed decays is estimated by the method of Ref. [33], which is controlled by the ratio of Cabibbo-suppressed and Cabibbo-favored rates combined with the strong phase difference between two amplitudes. The uncertainty is assigned to be 0.6%.

The uncertainties due to the limited MC statistics for various signal decays, (0.6–0.9)%, are taken into account as a systematic uncertainty. The uncertainties of the quoted branching fractions of the $K_S^0 \to \pi^+ \pi^-$ and $\pi^0 \to \gamma\gamma$ decays are 0.07% and 0.03%, respectively [12].

Table II summarizes the systematic uncertainties in the branching fraction measurements. For each signal channel, the total systematic uncertainty is obtained by adding the above sources quadratically. The obtained total systematic uncertainties are in the range of (3.0–5.8)% for various signal modes.

VIII. SUMMARY

In summary, we present the first measurements of the branching fractions of the hadronic decays of $D^0 \to K_S^0 \pi^0 \pi^0 \pi^0$, $D^0 \to K^- \pi^+ \pi^0 \pi^0 \pi^0$, $D^0 \to K_S^0 \pi^+ \pi^- \pi^0 \pi^0$,

TABLE III. Obtained BFs ($\mathcal{B}_{sig}$, $\mathcal{B}^{prd}_{D^{0(+)} \to \bar{K}\pi\eta}$, $\mathcal{B}^{prd}_{D^{0(+)} \to \bar{K}\pi\omega}$ and $\mathcal{B}_{non-\eta,\omega} = \mathcal{B}_{sig} - \mathcal{B}^{prd}_{D^{0(+)} \to \bar{K}\pi\eta} - \mathcal{B}^{prd}_{D^{0(+)} \to \bar{K}\pi\eta}$) for various signal decays (in units of 10^{-3}).

Decay mode	$\mathcal{B}_{sig}$	$\mathcal{B}^{prd}_{D^{0(+)} \to \bar{K}\pi\eta}$	$\mathcal{B}^{prd}_{D^{0(+)} \to \bar{K}\pi\omega}$	$\mathcal{B}_{non-\eta,\omega}$
$D^0 \to K_S^0 \pi^0 \pi^0 \pi^0$	$7.64 \pm 0.30 \pm 0.29$	1.66 ± 0.04	$\cdots$	$5.98 \pm 0.30 \pm 0.29$
$D^0 \to K^- \pi^+ \pi^0 \pi^0 \pi^0$	$9.54 \pm 0.30 \pm 0.31$	6.06 ± 0.13	$\cdots$	$3.48 \pm 0.30 \pm 0.34$
$D^0 \to K_S^0 \pi^+ \pi^- \pi^0 \pi^0$	$12.66 \pm 0.45 \pm 0.43$	2.31 ± 0.11	7.14 ± 0.47	$3.21 \pm 0.45 \pm 0.65$
$D^+ \to K_S^0 \pi^+ \pi^0 \pi^0$	$29.04 \pm 0.62 \pm 0.87$	$\cdots$	$\cdots$	$29.04 \pm 0.62 \pm 0.87$
$D^+ \to K_S^0 \pi^+ \pi^+ \pi^- \pi^0$	$15.28 \pm 0.57 \pm 0.60$	3.00 ± 0.11	6.29 ± 0.44	$5.99 \pm 0.57 \pm 0.75$
$D^+ \to K_S^0 \pi^+ \pi^0 \pi^0 \pi^0$	$5.54 \pm 0.44 \pm 0.32$	4.28 ± 0.16	$\cdots$	$1.26 \pm 0.44 \pm 0.36$
$D^+ \to K^- \pi^+ \pi^+ \pi^0 \pi^0$	$4.95 \pm 0.26 \pm 0.19$	$\cdots$	$\cdots$	$4.95 \pm 0.26 \pm 0.19$

$D^+ \to K_S^0 \pi^+ \pi^0 \pi^0$, $D^+ \to K_S^0 \pi^+ \pi^0 \pi^0 \pi^0$, $D^+ \to K^- \pi^+ \pi^+ \pi^0 \pi^0$, and $D^+ \to K_S^0 \pi^+ \pi^+ \pi^- \pi^0$. After subtracting the known branching fractions $\mathcal{B}^{\mathrm{prd}}_{D^{0(+)} \to \bar{K}\pi\eta}$ and $\mathcal{B}^{\mathrm{prd}}_{D^{0(+)} \to \bar{K}\pi\omega}$ for $D \to \bar{K}\pi\eta$ and $D \to \bar{K}\pi\omega$ from these decays, the residual branching fractions are summarized in the last columns of Table III. Here, $\mathcal{B}^{\mathrm{prd}}_{D^{0(+)} \to \bar{K}\pi\eta} = \mathcal{B}_{D^{0(+)} \to \bar{K}\pi\eta} \times \mathcal{B}_{\eta \to 3\pi}$, $\mathcal{B}^{\mathrm{prd}}_{D^{0(+)} \to \bar{K}\pi\omega} = \mathcal{B}_{D^{0(+)} \to \bar{K}\pi\omega} \times \mathcal{B}_{\omega \to 3\pi}$, and $\bar{K}$ denotes K_S^0 when a K_S^0 meson is involved in the decay. Except for the decay $D^+ \to K_S^0 \pi^+ \pi^0 \pi^0 \pi^0$, significant non-$(\eta, \omega)$ contributions have been found. In the near future, further amplitude analyses of these decays with larger data samples at BESIII [1] and Belle II [2] will provide rich information about the multibody hadronic D decays to scalar, vector, axial, and tensor mesons, which will benefit further understanding of quark SU(3)-flavor symmetry.

ACKNOWLEDGMENTS

[1] M. Ablikim *et al.* (BESIII Collaboration), Chin. Phys. C **44**, 040001 (2020).

[2] E. Kou *et al.* (Belle II Collaboration), Prog. Theor. Exp. Phys. **2019**, 123C01 (2019).

[3] R. Aaij *et al.* (LHCb Collaboration), arXiv:1808.08865.

[4] F. C. Adams and G. Laughlin, Rev. Mod. Phys. **69**, 337 (1997).

[5] W. Altmannshofer, P. Ball, A. Bharucha, A.-J. Buras, D. M. Straub, and M. Wick, J. High Energy Phys. 01 (2009) 019.

[6] M. Beneke, D. Boito, and Y. M. Wang, J. High Energy Phys. 11 (2014) 028.

[7] H. Y. Cheng and C. W. Chiang, Phys. Rev. D **81**, 074021 (2010).

[8] Q. Qin, H. N. Li, C. D. Lü, and F. S. Yu, Phys. Rev. D **89**, 054006 (2014).

[9] H. N. Li, C. D. Lü, and F. S. Yu, Phys. Rev. D **86**, 036012 (2012).

[10] H. Y. Cheng, Phys. Rev. D **67**, 094007 (2003); **68**, 014015 (2003); **67**, 034024 (2003).

[11] P. F. Guo, D. Wang, and F. S. Yu, Nucl. Phys. Rev. **36**, 125 (2019).

[12] P. A. Zyla *et al.* (Particle Data Group), Prog. Theor. Exp. Phys. **2020**, 083C01 (2020).

[13] M. Ablikim *et al.* (BESIII Collaboration), Chin. Phys. C **37**, 123001 (2013).

[14] M. Ablikim *et al.* (BESIII Collaboration), Phys. Lett. B **753**, 629 (2016).

[15] M. Ablikim *et al.* (BESIII Collaboration), Nucl. Instrum. Methods Phys. Res., Sect. A **614**, 345 (2010).

[16] C. Yu *et al.*, in proceedings of the *Proceedings of the 7th International Particle Accelerator Conference* (JACoW, Geneva, Switzerland, 2016), p. TUYA01, 10.18429/JA-CoW-IPAC2016-TUYA01.

[17] S. Agostinelli *et al.* (GEANT4 Collaboration), Nucl. Instrum. Methods Phys. Res., Sect. A **506**, 250 (2003).

[18] S. Jadach, B. F. L. Ward, and Z. Was, Comput. Phys. Commun. **130**, 260 (2000); Phys. Rev. D **63**, 113009 (2001).

[19] D. J. Lange, Nucl. Instrum. Methods Phys. Res., Sect. A **462**, 152 (2001); R. G. Ping, Chin. Phys. C **32**, 599 (2008).

[20] J. C. Chen, G. S. Huang, X. R. Qi, D. H. Zhang, and Y. S. Zhu, Phys. Rev. D **62**, 034003 (2000).

[21] R. L. Yang, R. G. Ping, and H. Chen, Chin. Phys. Lett. **31**, 061301 (2014).

[22] E. Richter-Was, Phys. Lett. B **303**, 163 (1993).

[23] R. M. Baltrusaitis *et al.* (MARK-III Collaboration), Phys. Rev. Lett. **56**, 2140 (1986).

[24] M. Ablikim *et al.* (BESIII Collaboration), Phys. Rev. D **100**, 072006 (2019).

[25] T.Gershon, J. Libby, and G. Wilkinson, Phys. Lett. B **750**, 338 (2015).

[26] M. Ablikim *et al.* (BESIII Collaboration), J. High Energy Phys. 05 (2021) 165.

[27] Heavy Flavor Averaging Group (HFLAV), http://www.slac.stanford.edu/xorg/hflav/charm/.

[28] M. Ablikim *et al.* (BESIII Collaboration), Eur. Phys. J. C **76**, 369 (2016).

[29] M. Ablikim *et al.* (BESIII Collaboration), Chin. Phys. C **40**, 113001 (2016).

[30] M. Ablikim *et al.* (BESIII Collaboration), Phys. Rev. Lett. **121**, 171803 (2018).

[31] M. Ablikim *et al.* (BESIII Collaboration), Phys. Lett. B **734**, 227 (2014).

[32] H. Albrecht *et al.* (ARGUS Collaboration), Phys. Lett. B **241**, 278 (1990).

[33] S. Dobbs *et al.* (CLEO Collaboration), Phys. Rev. D **76**, 112001 (2007).

[34] K. Stenson, arXiv:physics/0605236.

[35] M. Ablikim *et al.* (BESIII Collaboration), Phys. Rev. D **92**, 112008 (2015).